PCCP

Accepted Manuscript

ROYAL SOCIETY OF CHEMISTRY

www.rsc.org/pccp

PCCP

RSCPublishing

PAPER

Host-sensitized luminescence in $LaNbO_4:Ln^{3+}$ (Ln^{3+} = Eu^{3+}/Tb^{3+}/Dy^{3+}) with fruitful colors

Cite this: DOI: 10.1039/x0xx00000x

Kai Li,[a,b] Yang Zhang,[a,b] Xuejiao Li,[a] Mengmeng Shang,[a] Hongzhou Lian*[a] and Jun Lin*[a]

Received 00th January 2012,
Accepted 00th January 2012

DOI: 10.1039/x0xx00000x

www.rsc.org/

In this work, a series of Eu^{3+}, Tb^{3+}, and Dy^{3+} singly-doped and co-doped $LaNbO_4$ (LNO) phosphors have been synthesized by the high-temperature solid-state reaction route. X-ray diffraction (XRD) along with Rietveld refinement, diffuse reflection spectra, photoluminescence (PL) and cathodoluminescence (CL) properties, decay lifetimes, and PL quantum yields (QYs) were exploited to characterize the phosphors. Under UV excitation, there exists the energy transfer process from the host to the activators in singly-doped samples, which leads to the tunable emission color from blue to red for LNO:Eu^{3+}, green for LNO:Tb^{3+}, and yellow including white for LNO:Dy^{3+}. In Eu^{3+}, Tb^{3+} co-doped phosphors LNO: Eu^{3+}, Tb^{3+}, the energy transfers from the host to the activators and Tb^{3+} to Eu^{3+} ions have also been deduced from the PL spectra, resulting in the tunable emission color from green to red by adjusting the concentration ratio of Eu^{3+} and Tb^{3+} ions. The decay times monitored at host emission and Tb^{3+} emission confirm the existences of energy transfer in as-prepared samples. The best quantum efficiency can reach 43.2% for LNO:0.01Tb^{3+} in all as-prepared phosphors. On the other hand, the CL spectra of LNO:Eu^{3+}/Tb^{3+}/Dy^{3+} are a little different from their PL spectra because another emission envelope around 530 nm appears in samples, which is attributed to the higher energy excitation source of low-voltage electron beam bombardment. However, the characteristic emissions similar to PL spectra are reserved. Moreover, the CL spectrum of LNO:0.02Tb^{3+} has the stronger emission intensity than that of ZnO:Zn commercial product. These results in PL and CL properties of LNO:Eu^{3+}/Tb^{3+}/Dy^{3+} suggest their potential in solid-state lighting and display fields.

1. Introduction

In recent years, rare earth-doped inorganic luminescent materials have been extensively investigated and attracting much attention based on their wide applications in many lighting devices such as plasma display panels (PDPs), field emission displays (FEDs), liquid crystal displays (LCDs), light-emitting diodes (LEDs) and so on.[1] Among them, white LEDs have been regarded as the next promising generation of illumination source based on their superior merits of efficiently saving energy, being friendly to environment, high brightness, as well as long operation time compared with conventional incandescent and fluorescent lamps.[2] As to FEDs, their potentially superior characters in lighting, viewing, operated-temperature range, low consumption, response time, and so on impel them considered to be the next potentially technology in flat panel display.[3] As the indispensable and key components in the process of white LEDs and FEDs fabrication, the appropriate phosphors have been participating to be pursued in past and near future. Therefore, focusing interest on searching for highly efficient phosphors is highly desired for material researchers.

It is well known that introducing different rare earth ions into proper inorganic hosts as activators has been an usual method to obtain required phosphors based on 4f–4f or 4f–5d transitions of rare earth ions,[4] which can emit abundant colors upon their particular excitations. However, the intense host self-activated emissions without any rare earth ions doping can occur in several materials sometimes and they can effectively transfer their excitation energy to activators when introduced certain rare earth ions simultaneously. Therefore, host sensitization via energy transfer from the excited host to rare earth ions also becomes an effective route to enhance the emission intensity of activators. Eu^{3+}, the most common and widely used activator, can primarily emit red color originating from its characteristic transitional emissions of $^5D_{0,1,2}$-^7F_J (J = 4,…,0). As the green emission activator, Tb^{3+} has been broadly employed in many hosts based on its transitions of $^5D_4$-^7F_J (J = 3,4,5 and 6). Dy^{3+}-doped materials are often achieved as the white-emitting phosphors resulting from the combinational transitions of $^4F_{9/2}$-$^6H_{15/2}$ (blue) and $^4F_{9/2}$-$^6H_{13/2}$ (yellow) for Dy^{3+} ion.[5] Their emitting bands generally present several emission lines

[a]State Key Laboratory of Rare Earth Resource Utilization, Changchun Institute of Applied Chemistry, Chinese Academy of Sciences, Changchun 130022, People's Republic of China.
*E-mail: jlin@ciac.jl.cn, hzlian@ciac.jl.cn; Fax: +86-431-85698041; Tel: +86-431-85262031
[b]University of Chinese Academy of Sciences, Beijing 100049, People's Republic of China.

based on their 4f-4f spin-forbidden transitions which are not sensitive to the crystal fields around them in crystal lattices.

Niobates have been attracting a great deal of interest owing to their applications in a variety of devices such as non-linear optical crystal, single crystal fibers, photo-catalytic agent, as well as desired luminescent hosts.[6] $LaNbO_4$, a kind of niobate involving orthorhombic, monoclinic and tetragonal systems,[7] has been investigated as a luminescent material with the orthorhombic fergusonite structure, which shows an efficient blue luminescence upon both 254 nm UV excitation and X-ray sources.[6b,8] When sintered with $MoSi_2$, the obtained ceramic $LaNbO_4/MoSi_2$ has good hardness and high-melting-point. The addition of $LaNbO_4$ enhances the low-temperature flexibility of $MoSi_2$. Also, the good ionic and electronic conductivity in the $LaNbO_4$ system would make it a good candidate as the FED host material when doped into some rare earth ions because the emission intensity of cathodoluminescence (CL) depends on the conductivity of host when under a low voltage electron beam bombardment. However, the photoluminescence (PL) properties of Ln^{3+} doped well-crystallized monoclinic $LaNbO_4$ phosphors have rarely ever been investigated. In this work, we have synthesized a series of $Eu^{3+}/Tb^{3+}/Dy^{3+}$-doped $LaNbO_4$ and present the PL and CL properties of phosphors in detail, which exhibit different emission colors under UV radiation and a low voltage electron beam bombardment originating from the host sensitization of the NbO_4 group in the host to Ln^{3+} ions. Moreover, the crystal structural Rietveld refinement, the measurement of CIE chromaticity coordinates and the demonstrations of energy transfer mechanisms have been performed in detail in LNO: Ln^{3+} (Ln^{3+} = $Eu^{3+}/Tb^{3+}/Dy^{3+}$). The PL and CL properties of these phosphors we obtained suggest their potential applications in solid-state lighting and display fields.

2. Experimental section

2.1 Materials and preparation

A succession of phosphors with the chemical composition of $La_{1-x/y/z}NbO_4:xEu^{3+}/yTb^{3+}/zDy^{3+}$ (x = 0-0.10, y = 0-0.10, z = 0-0.08) where La atoms positions were considered to be occupied by rare earth atoms, were prepared through the conventional high-temperature solid-state reaction method. Typically, stoichiometric amounts of raw materials without any further purification, namely, Nb_2O_5 (A.R.), La_2O_3 (99.99%), Eu_2O_3 (99.99%), Tb_4O_7 (99.99%), Dy_2O_3 (99.99%) were utilized to thoroughly combined and ground in an agate mortar for about 15 min with an appropriate amount of ethanol followed by 5 min drying. After that, the powder mixtures were imbedded into the crucibles and transferred to the box furnace to anneal at 1400 °C for 7h in air condition to acquire the final samples after reground for 1 min.

2.2 Characterization

The D8 Focus diffractometer with graphite-monochromatized Cu Kα radiation (λ = 0.15405 nm) were used to obtain X-ray diffraction (XRD) patterns at the scanning rate of $10°min^{-1}$ in the 2θ range from 10° to 110°. The General Structure Analysis System (GSAS) program was availed to conduct the structure refinements. Diffuse reflectance spectral measurement was conducted with a Hitachi U-4100-Vis/NIR spectrophotometer. The PL spectra were recorded by a Hitachi F-7000 spectrophotometer with different excitation source (a 150 W xenon lamp and electron beam, respectively). The fluorescent decay curves were measured by a Lecroy Wave Runner 6100 Digital Osilloscope (1 GHz) using a tunable laser (pulse width = 4 ns, gate = 50 ns) as the excitation source (Contimuum Sunlite OPO). PL quantum yields (QYs) were obtained directly by the absolute PL quantum yield (internal quantum efficiency) measurement system (C9920-02, Hamamatsu Photonics K. K., Japan), involving an excitation light source of a Xe lamp, a monochromator, an integrating sphere capable of nitrogen gas flow, together with a CCD spectrometer for detecting the whole spectral range, simultaneously. All the measurements were carried out at room temperature (RT).

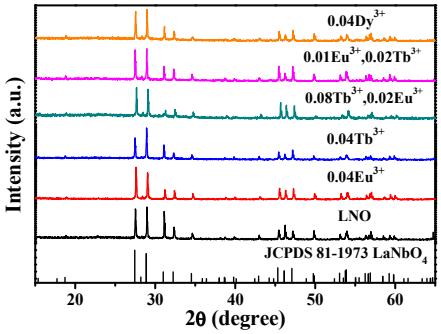

Fig. 1 XRD patterns for the representative LNO host, LNO:0.04Ln^{3+} (Ln^{3+} = $Eu^{3+}/Tb^{3+}/Dy^{3+}$), LNO:0.08Tb^{3+}, 0.02Eu^{3+} and LNO:0.01Eu^{3+}, 0.02Tb^{3+} samples，as well as the standard pattern (JCPDS 81-1973) of $LaNbO_4$.

3. Results and discussion

3.1 Phase identification and structure

Fig. 1 illustrates the representative XRD patterns of LNO host, LNO: 0.04Ln^{3+} (Ln^{3+} = $Eu^{3+}/Tb^{3+}/Dy^{3+}$), LNO: 0.08Tb^{3+}, 0.02Eu^{3+} and LNO:0.01Eu^{3+}, 0.02Tb^{3+} samples, which can reveal their chemical compositions and phases. All the diffraction peaks of obtained phosphors are well assigned to those of RT $LaNbO_4$ phase corresponding to the JCPDS Card no. 81-1973. No traces of other impurities are observed when doped with different Ln^{3+} ions, implying that the as-prepared samples crystallize in a single phase of $LaNbO_4$, and doping $Eu^{3+}/Tb^{3+}/Dy^{3+}$ ions into the hosts did not cause any significant transformation in the host structure. As depicted in Fig. 2, the RT $LaNbO_4$ phase crystallizes in monoclinic system with the space group of I12/c1(15) and cell parameters of a = 5.5647 Å, b = 11.5194 Å, c = 5.2015 Å, V = 332.57 $Å^3$, Z = 4,[9] which possesses a low-symmetry crystal structure, and the La atoms are at the center of the polyhedral surrounded by eight oxygen atoms. There is only one kind of La cationic site with Wyckoff position 4e for activators to accommodate attributed to their similar ionic radius of La^{3+} [r = 1.18 Å for coordination number (CN) = 8] and Eu^{3+} (r = 1.07 Å for CN = 8), Tb^{3+} (r = 1.04 Å for CN = 8), and Dy^{3+} (r = 1.02 Å for CN = 8). Although the phase transformation would like to proceed in $LaNbO_4$ from monoclinic to tetragonal when the temperature exceeds 520 °C,[6c] the high-temperature tetragonal phase could not ever be obtained with variously calcined temperature. In order to further identify the effect to crystal structure when doped rare earth ions, the crystal structure refinements of representative LNO host and LNO:0.04Ln^{3+} (Ln^{3+} = $Eu^{3+}/Tb^{3+}/Dy^{3+}$) samples were conducted by the general structure analysis system (GSAS) method. The refinement patterns of samples are presented in

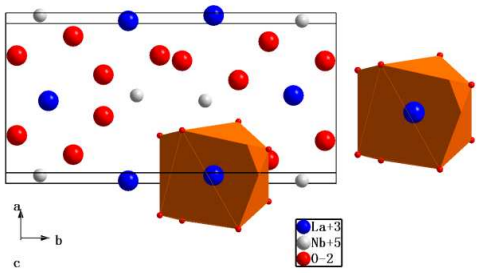

Fig. 2 Crystal structure of $LaNbO_4$ and coordination polyhedral of a representative La atom.

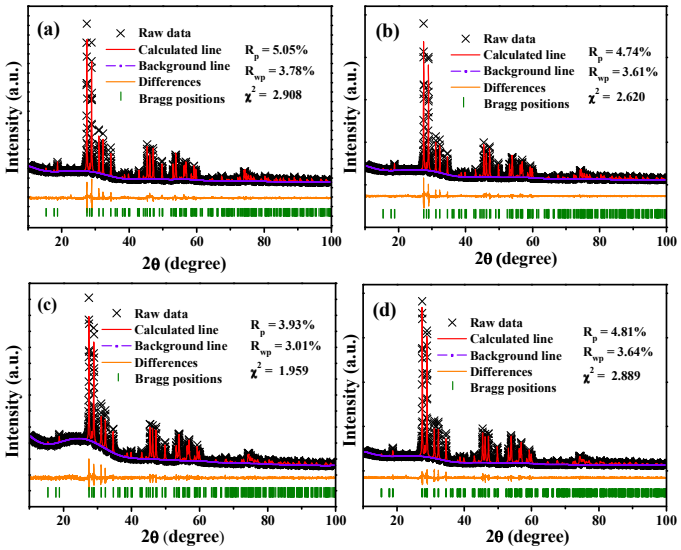

Fig. 3 The Rietveld refinements of powder XRD profiles of representative LNO host (a), LNO:0.04Eu^{3+} (b), LNO:0.04Tb^{3+} (c) and LNO:0.04Dy^{3+} (d) samples.

Fig. 3, and the detailed results are listed in Table 1. In the refinement process, the crystal data (ICSD #77390) is utilized as the original model. The experimental, calculated, and difference of XRD profiles and Bragg positions for the Rietveld refinements of LNO host and LNO:0.04Ln^{3+} (Ln^{3+} = Eu^{3+}/Tb^{3+}/Dy^{3+}) samples at RT are also shown in Fig. 3, which imply that doping Ln^{3+} ions into the host has little influence to the crystal structure of monoclinic $LaNbO_4$.

3.2 Photoluminescence properties

Fig. 4 shows the diffuse reflection spectra of LNO host, LNO:0.04Ln^{3+} (Ln^{3+} = Eu^{3+}/Tb^{3+}/Dy^{3+}) and LNO:0.08Tb^{3+}, 0.04Eu^{3+} samples, in which their profiles are similar, illustrating that the absorptions of dopant samples derive from the host. The reflectance spectra display strong energy absorption bands with the wavelength extent of 220-350 nm, corresponding to the charge transfer band (CTB) from O ligands to central Nb atoms in the NbO_4 tetrahedral groups. The absorption edge of this host from the reflectance spectra can be evaluated using the following Kubelka-Munk absorption coefficient (*K*/*S*) relationship:[10]

$$(1-R)^2 / 2R = K / S \quad (1)$$

where *K* represents the absorption coefficient, *R* refers to the reflectivity and *S* is the scattering coefficient. The optical band gap is evaluated to be 3.895 eV, which is in accordance with the PL excitation spectrum of the host in Fig. 5a. Fig. 5a illustrates the PL excitation and emission spectra of the LNO host. Upon 261 nm UV radiation n, a broad emission band peaked at 409 nm in the range of 320-550 nm can be observed. A wide excitation band around 261 nm with the wavelength extent of 200-300 nm can be found when detected at 409 nm. By and large, upon UV excitation, a great many electrons in the conduction band (CB) and free holes in the valance band (VB) can be respectively emerged. After that, the corresponding self-trapped holes (STHs) are rapidly engendered from the transformation of as-acquired free holes. However, some

Table 1 The final parameters for crystallography and detailed refinement results for LNO host and LNO: 0.04Ln^{3+} (Ln^{3+} = Eu^{3+}/Tb^{3+}/Dy^{3+}).

Formula	$LaNbO_4$	$La_{0.96}Eu_{0.04}NbO_4$	$La_{0.96}Tb_{0.04}NbO_4$	$La_{0.96}Dy_{0.04}NbO_4$
Crystal system	monoclinic	monoclinic	monoclinic	monoclinic
Space group	I12/c1	I12/c1	I12/c1	I12/c1
a/Å	5.5658(1)	5.5579(1)	5.5549(2)	5.5586(1)
b/Å	11.5256(1)	11.5080(1)	11.5044(3)	11.5124(2)
c/Å	5.2044(1)	5.2003(1)	5.1994(1)	5.2032(1)
V/Å^3	333.02(1)	331.78(1)	331.44(2)	332.13(1)
α = β/°	90	90	90	90
γ/°	94.07	94.08	94.07	94.07
Z	4	4	4	4
Radiation type	Cu-K_α	Cu-K_α	Cu-K_α	Cu-K_α
Wavelength/Å	1.5418	1.5418	1.5418	1.5418
Profile range/°	10-110	10-110	10-110	10-110
R_p/%	5.05	4.74	3.93	4.81
R_{wp}/%	3.78	3.61	3.01	3.64
χ^2	2.908	2.620	1.959	2.889

unsaturated atoms and unpaired electrons are generally positioned in the surface regions to generate many localized levels in the forbidden gaps. Some electrons are likely to be transited to these localized levels upon expected energy excitation, thus certain polarons as captured centers will appear and interact with the STHs to generate self-trapped excitons (STEs). At length, the recombination of these excitons leads to the broad emission band.[11] Fig. 5b presents the PL excitation and emission spectra of LNO:0.04Eu^{3+}. Monitored at 616 nm of Eu^{3+} characteristic emission peak, both a wide excitation band centered at 276 nm ranging from 200 to 320 nm and many excitation lines (362, 384, 396, 418, 467 and 540 nm, respectively) beyond 320 nm are observed, which correspond to the combinational CTB transitions of Eu^{3+}-O^{2-} and Nb^{5+}-O^{2-}, and Eu^{3+} 4f-4f characteristic transitions, respectively. Upon 261 nm UV excitation, both the host emission around 409 nm and Eu^{3+} 4f-4f characteristic transition emission lines appear, namely, $^5D_{0,1}$ excited states to the ^7F_J ground states including $^5D_1 \rightarrow {}^7F_1$ (540 nm), $^5D_0 \rightarrow {}^7F_1$ (595 nm), $^5D_0 \rightarrow {}^7F_2$ (616 nm) and $^5D_0 \rightarrow {}^7F_3$ (628 nm), respectively, in which the intensity of the electric dipole transition $^5D_0 \rightarrow {}^7F_2$ around 616 nm is much higher than that of the magnetic dipole $^5D_0 \rightarrow {}^7F_1$ around 593 nm, implying that the Eu^{3+} ions easily occupy the sites without or deviated from inversion symmetry. However, the Eu^{3+} 4f-4f transition emission lines also can be observed only at 396 nm UV excitation. Similarly, when Tb^{3+} or Dy^{3+} doped into hosts, not only the host emission but also the Tb^{3+}/Dy^{3+} 4f-4f transition emission lines [491 nm ($^5D_4 \rightarrow {}^7F_6$), 550 nm ($^5D_4 \rightarrow {}^7F_5$), 590 nm ($^5D_4 \rightarrow {}^7F_4$) and 623 nm ($^5D_4 \rightarrow {}^7F_3$) for Tb^{3+} ion, 487 nm ($^4F_{9/2} \rightarrow {}^6H_{15/2}$) and 578 nm ($^4F_{9/2} \rightarrow {}^6H_{13/2}$) for Dy^{3+} ion] can be clearly observed in Fig. 5c and e, respectively. Upon their respectively unique excitation at 380 and 353 nm, the Tb^{3+} or Dy^{3+} 4f-4f transition emission bands have their characteristic emission lines only. The emission intensities of doped Ln^{3+} 4f-4f transition excited at their different characteristic wavelengths are much weaker than that excited at CTB transition band of $O^{2-} \rightarrow Nb^{5+}$. Monitored at 550 nm, the profile of excitation spectrum except the excitation lines of Tb^{3+} beyond 320 nm in LNO:0.04Tb^{3+} has a little difference from the LNO one detected at 409 nm, which may attributed to the combination of Tb^{3+} 4f-5d transition and host CTB transition of Nb^{5+}-O^{2-}. However, the profile of excitation spectrum detected at 578 nm except the excitation lines of Dy^{3+} beyond 320 nm in LNO:0.04Dy^{3+} is identical with the LNO one monitored at 409 nm, which is originated from the Nb^{5+}-O^{2-} CTB transition of host only. Fig. 5d presents the PL excitation and emission spectra of Eu^{3+} and Tb^{3+} co-doped LNO:0.08Tb^{3+}, 0.02Eu^{3+} sample. Upon UV excitation into the NbO_4 group at 261 nm, the emission lines of Eu^{3+} and Tb^{3+} are both observed in the sample, which displays the combined emission color of red and green. Monitored at 550 and 616 nm, the excitation spectra are similar to that of LNO:0.04Tb^{3+} and LNO:0.04Eu^{3+}, respectively, however, the excitation lines of LNO:0.04Eu^{3+} beyond 300 nm involve the ones of LNO:0.04Tb^{3+}, which shows the possible existence of energy transfer from Tb^{3+} to Eu^{3+} in Eu^{3+} and Tb^{3+} co-doped LNO samples. Fig. 6 shows the decay curves of Ln^{3+} ions emissions (monitored at 616 nm for Eu^{3+}, 550 nm for Tb^{3+} and 578 nm for Dy^{3+}) in representative LNO:0.04Ln^{3+} (Ln^{3+} = Eu^{3+}/Tb^{3+}/Dy^{3+}) samples excited at 261 nm, they follow a non-exponential decay equation:[12]

$$I(t) = I_0 \exp\left[(-t/\tau) - (2bt^{1/2})\right] \quad (2)$$

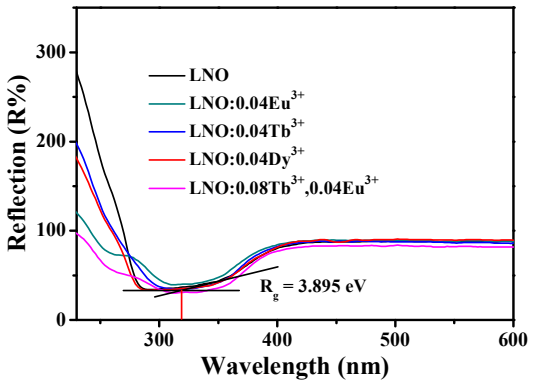

Fig. 4 Diffuse reflection spectra of LNO host, LNO:0.04Ln^{3+} (Ln^{3+} = Eu^{3+}/Tb^{3+}/Dy^{3+}) and LNO:0.08Tb^{3+}, 0.04Eu^{3+} samples.

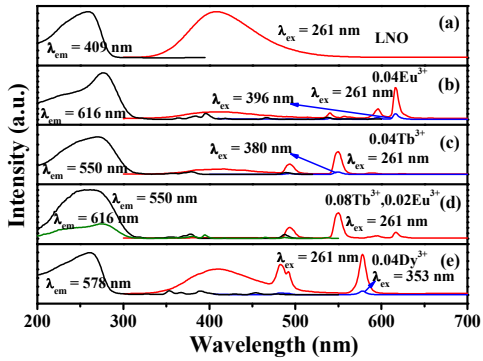

Fig. 5 PL excitation and emission spectra of the LNO host (a) , LNO:0.04Ln^{3+} (Ln^{3+} = Eu^{3+}/Tb^{3+}/Dy^{3+}) (b, c, e) and LNO:0.08Tb^{3+}, 0.02Eu^{3+} (d) samples.

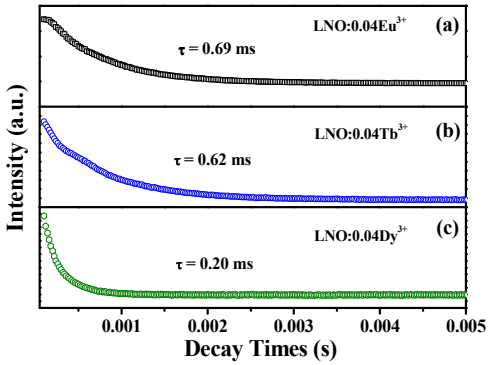

Fig. 6 Decay curves of Ln^{3+} ions in representative LNO:0.04Ln^{3+} (Ln^{3+} = Eu^{3+}/Tb^{3+}/Dy^{3+}) samples excited at 261 nm [monitored at 616 nm for Eu^{3+} (a), 550 nm for Tb^{3+} (b) and 578 nm for Dy^{3+} (c)].

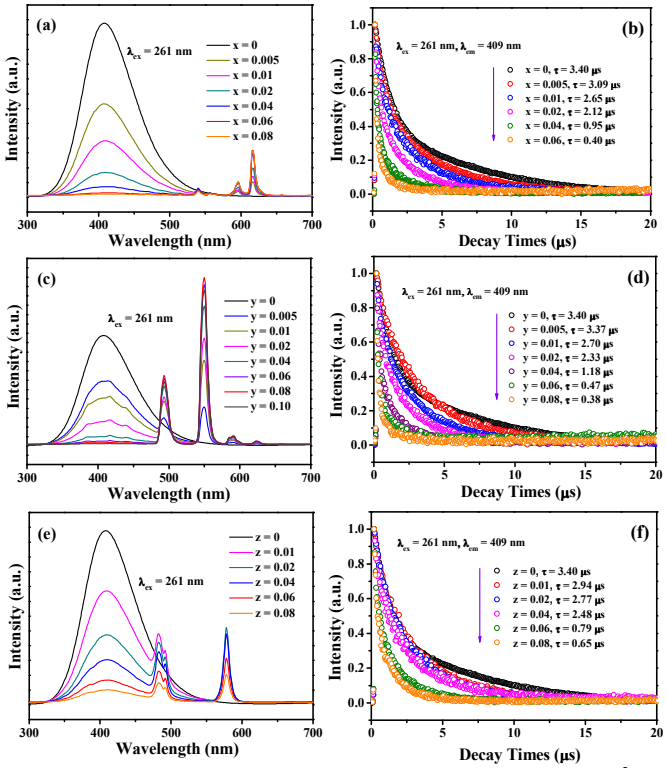

Fig. 7 Dependence of PL emission spectra of LNO:xEu^{3+} (a) /yTb^{3+} (c) /zDy^{3+} (e) on Ln^{3+} ions concentrations (x = 0-0.08, y = 0-0.10, z = 0-0.08) excited at 261 nm and their corresponding host emission decay times (monitored at 409 nm, excited at 261 nm) (b, d, f), respectively.

where I represents the fluorescent intensity, t is the time and τ corresponds to the decay lifetime for the exponential component, where b is quencher concentration as well as diffusion coefficient dependent. Assuming resonance energy transfer occurs in three dimensions, t has the powers of 1/2. The value of lifetimes are determined to be 0.69, 0.62 and 0.20 ms for Eu^{3+}, Tb^{3+} and Dy^{3+}, respectively, which are similar to the previous results in references[13] and much longer than that of the host emission (monitored at 409 nm) below in Fig. 7. These results illustrate that the Ln^{3+} ions can be accommodated into this kind of host and present their characteristic emission spectra.

The variations of emission spectra and host emissions decay curves as a function of concentration on Eu^{3+}/Tb^{3+}/Dy^{3+} in LNO:xEu^{3+}/yTb^{3+}/zDy^{3+} (x = 0-0.08, y = 0-0.10, z = 0-0.08) excited at 261 nm are shown in Fig. 7. With the increasing concentration on Eu^{3+}/Tb^{3+}/Dy^{3+} in single-doped samples, the intensity of host emission decreases monotonously, while the emission intensity of Eu^{3+}/Tb^{3+}/Dy^{3+} characteristic transitions first increases to a maximum corresponding to x = 0.06, y = 0.08 and z = 0.02, respectively, then decreases with further concentration attributed to the usual concentration quenching effect in Fig. 7a, c and e. This phenomenon can illustrate the existence of energy transfer process from the host to the activators in LNO:Eu^{3+}/Tb^{3+}/Dy^{3+} samples. The decay times of host emissions decrease monotonously with the increases of Ln^{3+} ions concentration. They can be approximately calculated using the equation 2, which decrease monotonously from 3.40 μs to 0.40/0.38/0.65 μs. The declined decay times give further confirmations of energy transfer from the host to the activators in LNO:Eu^{3+}/Tb^{3+}/Dy^{3+} phosphors.

The energy transfer efficiency (η_T) from the host to the Ln^{3+} ions in LNO: xEu^{3+}/yTb^{3+}/zDy^{3+} systems can be approximately calculated utilizing the formula $\eta_T = 1-I_S/I_{S0}$,[14] where η_T is the energy transfer efficiencies, and I_{S0} and I_S correspond to the luminescence intensities of the host with the presence and absence of an activator (Eu^{3+}/Tb^{3+}/Dy^{3+}), respectively. As illustrated in Fig. 8, the various values of η_T are plotted as a function of concentration of Eu^{3+}/Tb^{3+}/Dy^{3+} ions, which depict that the η_T values gradually increase to reach maximums at 98.23%, 97.92% and 91.44% without saturation when using 261 nm UV as the excited wavelength, respectively, indicating the energy transfer from the NbO_4 group in the host to the activators becomes more and more efficient with the raise of Eu^{3+}/Tb^{3+}/Dy^{3+} ions concentration.

3.3 Energy transfer mechanisms

In order to deduce the energy transfer mechanisms from the host to the activators in LNO:xEu^{3+}/yTb^{3+}/zDy^{3+} system, the critical distances (R_c) between activators such as Eu^{3+}/Tb^{3+}/Dy^{3+} here are of importance to be determined, which can be gained roughly evaluated by the equation proposed by Blasse:[15]

$$R_c = 2\left(\frac{3V}{4\pi X_c N}\right)^{1/3} \quad (3)$$

where V represents the volume of the unit cell, N is the number of host cations in the unit cell, and X_c refers to the critical concentration of dopant ions. For the LNO host, N = 4, V = 332.57 Å^3, and X_c corresponds to 6%, 8% and 2% for Eu^{3+}, Tb^{3+} and Dy^{3+}, respectively; Consequently, the R_c were estimated to be about 13.83, 12.57 and 19.95 Å. It is well known that the probability of energy migration from the host to the activators rises with the increasing Eu^{3+}/Tb^{3+}/Dy^{3+} content. When the distance reaches small enough, the concentration quenching phenomenon occurs and the energy migration is hindered.

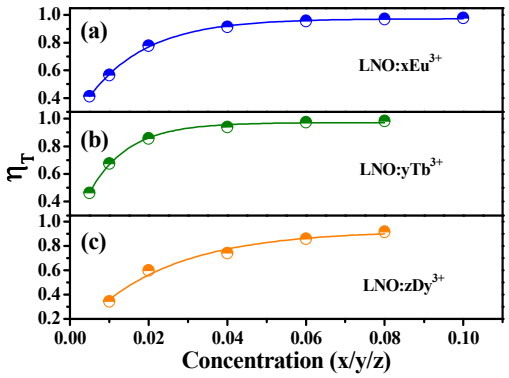

Fig. 8 Energy transfer efficiencies (η_T) from the host to the activators in LNO:xEu^{3+} (a), LNO:yTb^{3+} (b), LNO:zDy^{3+} (c).

Frequently, exchange interaction, radiation reabsorption and electric multipolar interactions are the three mechanisms for non-radiate energy transfer process. The values of R_c acquired above imply the little possibility of exchange interaction since it can be predominant only for about 5 Å.[16] Another mechanism of radiation reabsorption becomes dominant only when the from the host to the activators. Based on Dexter's energy transfer formula of multipolar interactions and Reisfeld's approximation, the following relationship can be attained:[16a,17]

$$\frac{\eta_{S0}}{\eta_S} \propto C^{\alpha/3} \quad (4)$$

where η_{S0} and η_S correspond to the luminescence quantum efficiencies of the host with the absence and presence of the $Eu^{3+}/Tb^{3+}/Dy^{3+}$ ions, respectively. C is the concentration of the $Eu^{3+}/Tb^{3+}/Dy^{3+}$ ions. The value for α = 6, 8, and 10 corresponds to dipole-dipole, dipole-quadrupole, and quadrupole-quadrupole interactions, respectively. Generally, the value of η_{S0}/η_S is not easy to be obtained and thus often approximately calculated using the I_{S0}/I_S, where I_{S0} and I_S stand for the luminescence intensity of the host without and with the $Eu^{3+}/Tb^{3+}/Dy^3$ ions, respectively, the following expression can be obtained:[18]

$$\frac{I_{S0}}{I_S} \propto C^{\alpha/3} \quad (5)$$

The relationship between I_{S0}/I_S and $C^{\alpha/3}$ according to the above equation are illustrated in Fig. 9. All the linear relationships are only found when α = 6. As a result, this indicates the energy transfer from the host to $Eu^{3+}/Tb^{3+}/Dy^{3+}$ ions proceeds through the dipole-dipole mechanisms in LNO:$Eu^{3+}/Tb^{3+}/Dy^{3+}$ phosphors, respectively.

The emission spectra excited at 261 nm of Tb^{3+}, Eu^{3+} co-doped LNO samples LNO:0.08Tb^{3+}, xEu^{3+} and LNO:0.02Eu^{3+}, yTb^{3+} are depicted in Fig. 10a and c when the content of Tb^{3+} and Eu^{3+} are fixed at y = 0.08 and x = 0.01, respectively. We can observe that the intensity of Tb^{3+} emission in LNO:0.08Tb^{3+}, xEu^{3+} descends monotonously with the increment of Eu^{3+} content, whereas the emission intensity of Eu^{3+} first increases until the concentration saturation of Eu^{3+} ions at x = 0.06, which illustrates the energy transfer from Tb^{3+} to Eu^{3+} ions can take place. The decline of the emission intensity should be ascribed to the conventional concentration quenching effect, which often occurs in phosphors. In LNO: 0.02Eu^{3+}, yTb^{3+}, the host emission intensity descends monotonously while the emission intensity of Tb^{3+} ascends monotonously in our prepared samples with the increment of Tb^{3+} concentration. However, the intensity of Eu^{3+} emission varies little. The result proposes that the energy transfer from the host to Tb^{3+} is prior to that from Tb^{3+} to Eu^{3+} ions in these samples. The declined decay times for Tb^{3+} emission in LNO:0.08Tb^{3+}, xEu^{3+} and host emission in LNO:0.02Eu^{3+}, yTb^{3+} indicate the occurrence of energy transfer process from Tb^{3+} to Eu^{3+} ions and the host to Tb^{3+} ions in Fig. 10b and d, respectively.

The detailed values of PL quantum efficiencies (QYs) and corresponding variations of CIE chromaticity (Commission Internationale de I'Eclairage 1931 chromaticity) coordinates for as-prepared LNO:$Eu^{3+}/Tb^{3+}/Dy^{3+}$ samples upon 261 nm UV excitation have been listed in Table 2. We can observe the value of QY for LNO host is measured to be 41.0%. With the increasing activators concentrations, the maximum value of QY can reach 41.9% for LNO:0.005Eu^{3+}, 43.2% for LNO:0.01Tb^{3+} and 40.5% for LNO:0.01Dy^{3+}. In Eu^{3+}, Tb^{3+} co-doped LNO samples, the maximum QY is 35.3% for LNO:0.01Eu^{3+}, 0.06Tb^{3+}. However, the QY can be improved via controlling the particle size, morphology, and crystalline defects with the optimizations of the synthesis processing and chemical composition. The CIE chromaticity coordinates of LNO:$Eu^{3+}/Tb^{3+}/Dy^{3+}$ phosphors upon 261 nm UV excitation can vary from (0.151, 0.041) for LNO host to (0.667, 0.333) for LNO:0.10Eu^{3+}, (0.313, 0.627) for LNO:0.10Tb^{3+}, and (0.462, 0.496) for LNO:0.08Dy^{3+}, which correspond to the color tunes from blue to red, green, and yellow, respectively. Especially, the CIE chromaticity coordinates of LNO:0.04Dy^{3+} is (0.341, 0.326), which is very close to the standard value of white emission (0.333, 0.333). In LNO:0.08Tb^{3+}, xEu^{3+} phosphors, the CIE chromaticity coordinate varies from (0.313, 0.627) to(0.646, 0.354) corresponding to x = 0 and 0.08, respectively. In LNO:0.01Eu^{3+}, yTb^{3+} phosphors, the CIE coordinate shifts from (0.534, 0.245) to (0.387, 0.567) corresponding to y = 0 and 0.06, respectively. The variety of CIE chromaticity coordinates of as-prepared samples excited at 261 nm and digital luminescence photographs upon a 254 nm UV lamp

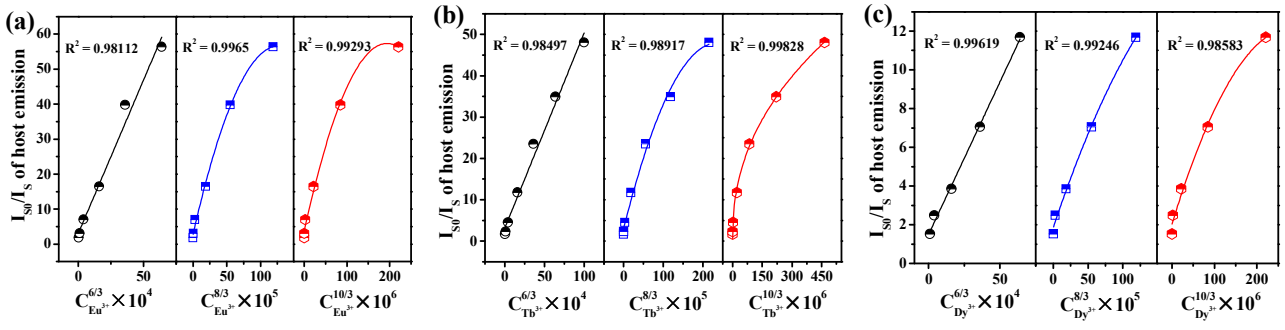

Fig. 9 Dependence of I_{S0}/I_S of host emission on $C^{6/3}$, $C^{8/3}$, and $C^{10/3}$ in LNO:$Eu^{3+}/Tb^{3+}/Dy^{3+}$ (a-c), respectively.

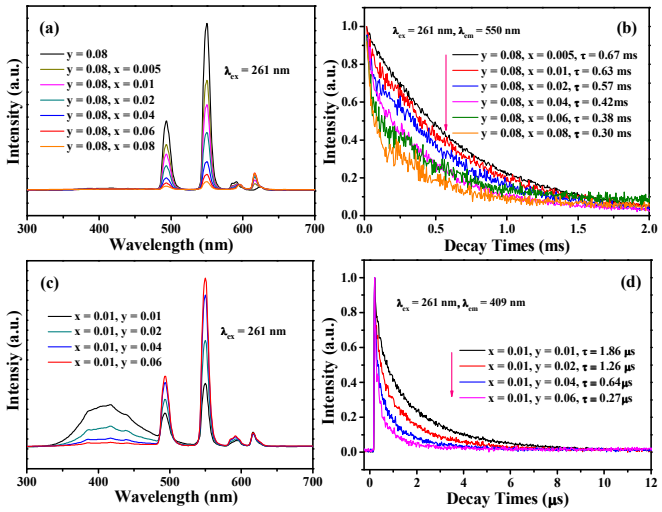

Fig. 10 Dependences of PL emission spectra and corresponding decay times on Eu^{3+} (monitored at 550 nm) or Tb^{3+} (monitored at 409 nm) concentration under 261 nm UV radiation in LNO:0.08Tb^{3+}, xEu^{3+} (a and b) and LNO:0.01Eu^{3+}, yTb^{3+} (c and d)phosphors (x = 0-0.08, y = 0.01-0.06).

excitation are presented in Fig. 11, respectively, which indicate the tunable color can be realized via doping different activators and their concentrations.

3.4 Cathodoluminescence properties

In order to examine the potential application of as-prepared LNO:Eu^{3+}/Tb^{3+}/Dy^{3+} phosphors as the candidates for field emission materials, their CL properties have been investigated in detail. As depicted in Fig. 12, the typical CL spectra together with the corresponding digital luminescence photographs of LNO host and LNO:Eu^{3+}/Tb^{3+}/Dy^{3+} phosphors have been clearly observed under low-voltage electron-beam excitation (accelerating voltage = 4 kV, filament current = 90 mA). Compared with the PL spectra, the CL spectra have a little difference, namely, a new emission envelope around 530 nm appears in all the as-prepared samples. This can be explained by the fact that the electron beam has relative high energy and it may excite the electrons which can't be pumped by UV radiation for LNO host. For CL, the primary fast and energetic electrons produce many secondary electrons with a very wide excitation energy distribution. These electrons may excite the NbO_4 group in host lattice and create many electron–hole pairs, resulting in the formation of bound excitons. These excitons decay can transit from trap and defect level to valance band, giving their different emissions. However, the characteristic emissions of Eu^{3+}/Tb^{3+}/Dy^{3+} and LNO emission band around 409 nm similar to PL spectra have been reserved in LNO:Eu^{3+}/Tb^{3+}/Dy^{3+} phosphors, which make them present different emission colors (red for LNO:0.04Eu^{3+}, green for LNO:0.02Tb^{3+}, white for LNO:0.04Dy^{3+}) via the energy transfer from the host to the activators under low-voltage electron-beam excitation. Fig. 13 presents the CL spectra for LNO:yTb^{3+} (y = 0.005-0.08) as the representative samples

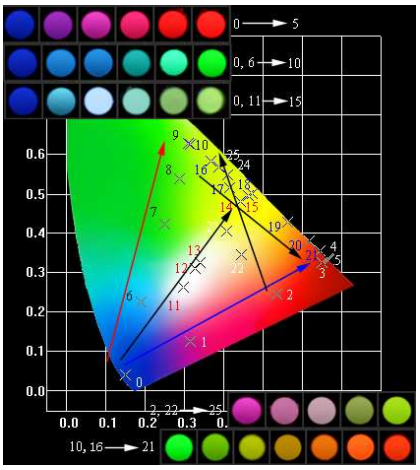

Fig. 11 The variety of CIE chromaticity coordinate of as-prepared samples excited at 261 nm and the digital luminescence photographs under a 254 nm UV lamp excitation, respectively.

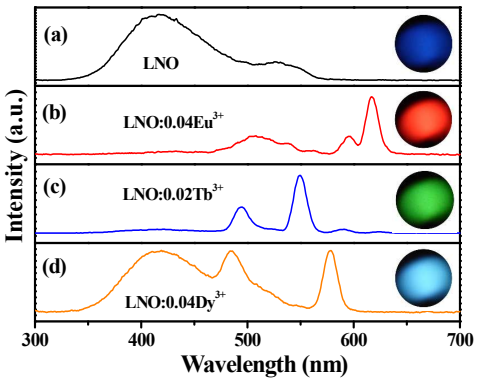

Fig. 12 CL spectra for LNO host (a), LNO:0.04Eu^{3+} (b), LNO:0.02Tb^{3+} (c), LNO:0.04Dy^{3+} (d) with corresponding digital luminescent photographs on the right under low-voltage electron beam excitation.

under low-voltage electron beam excitation with the accelerating voltage of 3 kV and filament current of 90 mA to validate the existence of energy transfer from the host to the activators in LNO:Eu^{3+}/Tb^{3+}/Dy^{3+} phosphors. One can find that the emission intensity of LNO monotonously decreases while the Tb^{3+} emission intensity of $^5D_4 \rightarrow {}^7F_5$ transition at 550 nm increases to a maximum at y = 0.02 and subsequently descends with further concentration of Tb^{3+}, demonstrating the energy transfer from the host to the Tb^{3+} ions. It is well accepted that the commercial ZnO:Zn displays bright green luminescence and has been confirmed to be a potential phosphor for FEDs application under low-voltage electron-beam excitation. Fig. 14 shows the comparison of CL spectra as well as digital luminescent photographs of ZnO:Zn and LNO:0.02Tb^{3+} under low-voltage electron beam excitation with the filament current of 90 mA and accelerating voltage of 3 kV. As to CL, the emission band areas (integrated luminescence intensity) and the CL intensity (in height) are used to roughly assess the

efficiency of a luminescent material containing the radiant efficiency (η) and the luminous efficiency (L, brightness),[19] respectively. It can be clearly found the emission band area of the LNO:0.02Tb^{3+} is smaller than that of ZnO:Zn, however, the accelerating voltage of 3 kV, the CL emission intensities of phosphors raise monotonously (Fig. 15b). There is not any saturation effect for the CL intensity of these samples with the increment of filament current and accelerating voltage. This indicates that the phosphors are resistant to the current CL intensity of as-synthesized LNO:0.02Tb^{3+} (in height) can be stronger than that of ZnO:Zn, which suggest it a promising candidate for FEDs phosphor.

Fig. 15 plots the variation of CL intensities of representative LNO:0.04Eu^{3+}, LNO:0.02Tb^{3+}, LNO: 0.04Dy^{3+} samples as a function of accelerating voltage and filament current in detail, respectively. At a stationary filament current of 90 mA, the

Table 2 Variation of quantum Yields (QYs) and corresponding variations of CIE chromaticity coordinate for LNO:Eu^{3+}/Tb^{3+} /Dy^{3+} phosphors excited under 261 nm UV radiation.

No. of points	LNO:xEu^{3+}/yTb^{3+}/zDy^{3+}	QYs/%	CIE (x, y)
0	x = 0	41.0	(0.151, 0.041)
1	x = 0.005	41.9	(0.314, 0.124)
2	x = 0.01	28.2	(0.534, 0.245)
3	x = 0.02	32.9	(0.649, 0.326)
4	x = 0.06	36.9	(0.664, 0.336)
5	x = 0.10	37.1	(0.667, 0.333)
6	y = 0.005	40.5	(0.190, 0.225)
7	y = 0.01	43.2	(0.249, 0.422)
8	y = 0.02	41.4	(0.288, 0.538)
9	y = 0.04	41.3	(0.311, 0.627)
10	y = 0.08	38.6	(0.313, 0.627)
11	z = 0.01	40.5	(0.297, 0.262)
12	z = 0.02	39.9	(0.328, 0.309)
13	z = 0.04	34.5	(0.341, 0.326)
14	z = 0.06	15.5	(0.443, 0.481)
15	z = 0.08	10.9	(0.462, 0.496)
No. of points	**LNO:0.08Tb^{3+}, xEu^{3+}**	**QYs/%**	**CIE (x, y)**
10	x = 0	38.6	(0.313, 0.627)
16	x = 0.005	36.0	(0.368, 0.582)
17	x = 0.01	35.1	(0.415, 0.545)
18	x = 0.02	30.0	(0.473, 0.500)
19	x = 0.04	24.7	(0.562, 0.428)
20	x = 0.06	23.6	(0.617, 0.381)
21	x = 0.08	22.2	(0.646, 0.354)
No. of points	**LNO:0.01Eu^{3+}, yTb^{3+}**	**QYs/%**	**CIE (x, y)**
2	y = 0	28.2	(0.534, 0.245)
22	y = 0.005	29.3	(0.446, 0.344)
23	y = 0.01	29.3	(0.407, 0.404)
24	y = 0.02	31.9	(0.411, 0.547)
25	y = 0.06	35.3	(0.387, 0.567)

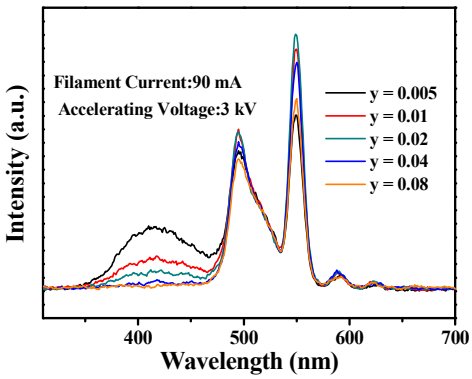

Fig. 13 Variation of CL spectra for LNO:yTb^{3+} (y = 0.005-0.08) phosphors under low-voltage electron beam excitation with the accelerating voltage of 3 kV and filament current of 90 mA.

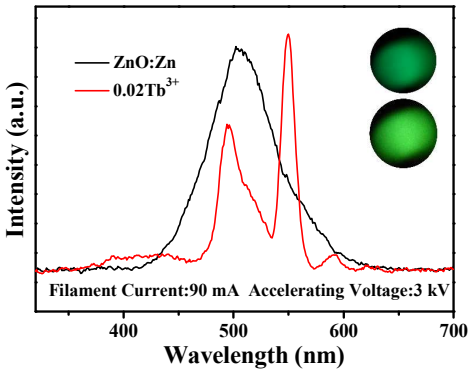

Fig. 14 CL spectra of ZnO:Zn and LNO:0.02Tb^{3+} under low-voltage electron beam excitation with the accelerating voltage of 3 kV and filament current of 90 mA. The inset is the digital luminescent photograph for the phosphors.

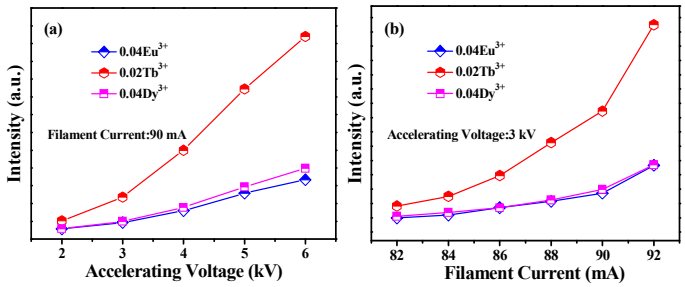

Fig. 15 The CL intensities of LNO:0.04Eu^{3+}, LNO:0.02Tb^{3+} and LNO:0.04Dy^{3+} samples as a function of (a) accelerating voltage and (b) filament current.

CL intensities of phosphors increase with the increment of accelerating voltage from 2 to 6kV (Fig. 15a). Similarly, with the increasing filament current from 82 to 92 mA at an aptotic saturation and have good conductivity, which are important for FED application. The raise in CL brightness with an increase in accelerating voltage and filament current can be attributed to the deeper penetration of the electrons into the phosphors body along with the larger electron-beam current density. The electron penetration depth can be estimated exploiting the empirical expression L [Å] = 250(A/ρ)($E/Z^{1/2}$)^{n}, where n =

$1.2/(1 - 0.29 \log_{10} Z)$,[20] A refers to the atomic or molecular weight of the material, ρ corresponds to the bulk density, Z represents the atomic number or the number of electrons per molecule in the case compounds, and E is the accelerating voltage (kV). For $LaNbO_4$, Z = 130, A = 295.81, ρ = 5.907g/cm^3. Therefore, the electron penetration depth are estimated to be 199.26, 486.25 and 971.37 nm corresponding to the accelerating voltage of 3, 4, 5 kV according to the above equation, respectively. For CL, the Eu^{3+}, Tb^{3+}, and Dy^{3+} ions are excited by the plasma generated by the incident electrons. The deeper the electron penetration depth, the more plasma will be produced, which induces more Eu^{3+}, Tb^{3+} and Dy^{3+} ions being excited, resulting in the increase of CL intensity.

4. Conclusions

In summary, a series of Eu^{3+}, Tb^{3+}, and Dy^{3+} singly-doped and co-doped LNO:Eu^{3+}/Tb^{3+}/Dy^{3+} phosphors have been synthesized by the high-temperature solid-state reaction method. Under UV excitation, the LNO host can emit an intense blue light. When Eu^{3+}/Tb^{3+}/Dy^{3+} were singly doped into host, the tunable emission colors occur based on the energy transfer from the host to the activators. The maximum quantum efficiency can reach 43.2% for LNO:0.01Tb^{3+} in all as-prepared samples. The energy transfer can be demonstrated by the variations of emission spectra and the decay times of host emissions with the increasing activators concentrations. Moreover, the Eu^{3+}, Tb^{3+} co-doped samples present tunable emission color from green to red by adjusting the concentration ratio of Eu^{3+} and Tb^{3+} ions. Under low-voltage electron beam bombardment, the CL spectra of LNO:Eu^{3+}/Tb^{3+}/Dy^{3+} indicate that they show a little difference from PL spectra because of the appearance of another emission envelope around 530 nm compared to PL spectra. However, they can also display intense tunable emission colors. In addition, the CL intensity of LNO:0.02Tb^{3+} is stronger than that of the ZnO:Zn commercial product under the same excitation condition. These results show that the as-prepared LNO:Eu^{3+}/Tb^{3+}/Dy^{3+} have the potential as the LEDs and FEDs phosphors.

Acknowledgments

This project is financially supported by the National Natural Science Foundation of China (NSFC Grants 51332008, 51172227, 91433110 and 21221061), National Basic Research Program of China (Grants 2014CB643803), and Joint Funds of the National Natural Science Foundation of China (Grant U13012038).

References

1 (a) Y. Liu, D. Tu, H. Zhu and X. Chen, *Chem. Soc. Rev*., 2013, **42**, 6924; (b) S.-S. Wang, W.-T. Chen, Y. Li, J. Wang, H.-S. Sheu and R.-S. Liu, *J. Am. Chem. Soc*., 2013, **135**, 12504; (c) R.-J. Xie, N. Hirosaki, M. Mitomo, Y. Yamamoto, T. Suehiro and K. Sakuma, *J. Phys. Chem. B*, 2004, **108**, 12027; (d) Q. Dai, M. E. Foley, C. J. Breshike, A. Lita and G. F. Strouse, *J. Am. Chem. Soc*., 2011, **133**, 15475; (e) X. Liu, C. Li, Z. Quan, Z. Cheng and J. Lin, *J. Phys. Chem. C*, 2007, **111**, 16601; (f) J. K. Park, K. J. Choi, J. H. Yeon, S. J. Lee and C. H. Kim, *Appl. Phys. Lett*., 2006, **88**, 043511.

2 (a) Y. S. Liu, D. T. Tu, H. M. Zhu, R. F. Li, W. Q. Luo and X. Y. Chen, *Adv. Mater*., 2010, **22**, 3266; (b) R. J. Xie, N. Hirosaki, T. Suehiro, F. F. Xu and M. Mitomo, *Chem. Mater*., 2006, **18**, 5578; (c) T. S. Chan, R. S. Liu and I. Baginskiy, *Chem. Mater*., 2008, **20**, 1215; (d) W.-R. Liu and P.-C. Lin, *OPTICS EXPRESS*, 2014, **22**, A446.

3 (a) Y. B. Mao, T. Tran, X. Guo, J. Y. Huang, C. K. Shih, K. L. Wang and J. P. Chang, *Adv. Funct. Mater*., 2009, **19**, 748; (b) N. Zhang, C. Guo and H. Jing, *RSC Adv*., 2013, **3**, 7495; (c) X. Liu, Y. Liu, D. Yan, H. Zhu, C. Liu, W. Liu, C. Xu, Y. Liu, H. Zhang and X. Wang, *Dalton Trans*., 2013, **42**, 16311; (d) M. Shang, D. Geng, D. Yang, X. Kang, Y. Zhang and J. Lin, *Inorg. Chem*., 2013, **52**, 3102. (e) J. Hao and M. Cocivera, *Appl. Phys. Lett.*, 2002, **81**, 4154.

4 (a) Y. Liu, X. Zhang, Z. Hao, X. Wang and J. Zhang, *Chem. Commun*., 2011, **47**, 10677; (b) K.-W. Huang, W.-T. Chen, C.-I. Chu, S.-F. Hu, H.-S. Sheu, B.-M. Cheng, J.-M. Chen and R.-S. Liu, *Chem. Mater*., 2012, **24**, 2220; (c) X. Zhang, C. Zhou, J. Song, L. Zhou and M. Gong, *J. Alloys Compd*., 2014, **592**, 283; (d) D. Kim, J. Jang, S. Ahn, S.-H. Kim and J.-C. Park, *J. Mater. Chem. C*, 2014, **2**, 2799.

5 (a) Y. Deng, S. Yi, J. Huang, J. Xian and W. Zhao, *Mater. Res. Bull*., 2014, **57**, 85; (b) D. Wen and J. Shi, *Dalton Trans*., 2013, **42**, 16621; (c) X. Yu, L. Zhang, X. Xu, T. Wang, H. Yu, T. Jiang, Q. Jiao, Z. Yang, D. Zhou and J. Qiu, *J. Lumin*., 2014, **145**, 114.

6 (a) L. T. Francis, P. P. Rao, M. Thomas, S. K. Mahesh, V. R. Reshmi and V. D. S. Thampi, *Mater. Lett*., 2012, **81**, 142; (b) G. Blasse and A. Bril, *J. Lumin*., 1970, **3**, 109; (c) G. Blasse and L. H. Brixner, *Chem. Phys. Lett*., 1990,**173**, 409.

7 (a) L. Jian, C. M. Huang, G. B. Xu and C. M. Wayman, *Mater. Lett*., 1994, **21**, 105; (b) L. Jian and C. M. Wayman, *J. Am. Ceram. Soc*., 1997, **80**, 803.

8 Y. Lv, X. Tang, L. Yan, K. Li, X. Liu, M. Shang, C. Li and J. Lin, *J. Phys. Chem. C*, 2013, **117**, 21972.

9 S. Tsunekawa, T. Kamiyama, K. Sasaki, H. Asano and T. Fukuda, *Acta Crystallogr., Sec. A: Found. Crystallogr*., 1993, 49595.

10 (a) Y. Zhang, D. Geng, X. Li, J. Fan, K. Li, H. Lian, M. Shang and J. Lin, *J. Phys. Chem. C*, 2014, **118**, 17983; (b) Z. Xia, J. Zhou and Z. Mao, *J. Mater. Chem. C*, 2013, **1**, 5917; (c) J. Sun, Z. Lian, G. Shen and D. Shen, *RSC Adv*., 2013, **3**, 18395.

11 Q. Ma, M. Lu, P. Yang, A. Zhang and Y. Cao, *Mater. Res. Bull*., 2013, **48**, 3677.

12 (a) R. Okram, N. Yaiphaba, R. S. Ningthoujam and N. Rajmuhon Singh, *Inorg. Chem*., 2014, **53**, 7204; (b) N. K. Sahu, N. S. Singh, R. S. Ningthoujam and D. Bahadur, *ACS Photonics*, 2014, **1**, 337.

13 (a) N. Niu, P. Yang, W. Wang, F. He, S. Gai, D. Wang and J. Lin, *Mater. Res. Bull*., 2011, **46**, 333; (b) A. A. Reddy, S. Das, A. Goel, R. Sen, R. Siegel, L. Mafra, G. Vijaya Prakash and J. M. F. Ferreira, *AIP ADVANCES*, 2013, **3**, 022126.

14 (a) Z. Xia, J. Zhuang, A. Meijerink and X. Jing, *Dalton Trans*., 2013, **42**, 6327; (b) J. Zhong, W. Zhao, L. Lan, J. Wang, J. Chen and N. Wang, *J. Alloys Compd*., 2014, **592**, 213; (c) S. Hu and W. Tang, *J. Lumin*., 2014, **145**, 100; (d) H. Liu, L. Liao and Z. Xia, *RSC Adv*., 2014, **4**, 7288. (e) Dimple P. Dutta, R. S. Ningthoujam and A. K. Tyagi, *AIP Advances*, 2012, **2**, 042184.

15 (a) G. Blasse, *J. Solid State Chem*., 1986, **62**, 207; (b) W.-R. Liu, C.-H. Huang, C.-W. Yeh, J.-C. Tsai, Y.-C. Chiu, Y.-T. Yeh and R.-S. Liu, *Inorg. Chem*., 2012, **51**, 9636; (c) Y.-C. Chiu, C.-H. Huang, T.-J. Lee, W.-R. Liu, Y.-T. Yeh, S.-M. Jang and R.-S. Liu, *OPTICS EXPRESS*, 2011, **19**, A331.

16 (a) D. L. Dexter, *J. Chem. Phys*., 1953, **21**, 836; (b) Z. Xia, R.-S. Liu, K.-W. Huang and V. Drozd, *J. Mater. Chem*., 2012, **22**, 15183.

17 (a) D. Wen, Z. Dong, J. Shi, M. Gong and M. Wu, *ECS J. Solid State Sci. and Tech*., 2013, **2(9)**, R178; (b) Z. Xia and R.-S. Liu, *J. Phys. Chem. C*, 2012, **116**, 15604.

18 (a) P. I. Paulose, G. Jose, V. Thomas, M. N. V. Unnikrishnan, K. R. Warrier, *J. Phys. Chem. Solids*, 2003, **64**, 841; (b) D. L. Dexter and J. A. Schulman, *J. Chem. Phys*., 1954, **22**, 1063; (c) C.-H. Huang, T.-S. Chan, W.-R. Liu, D.-Y. Wang, Y.-C. Chiu, Y.-T. Yeh and T.-M. Chen, *J. Mater. Chem*., 2012, **22**, 20210–20216.

19 (a) D. Geng, G. Li, M. Shang, C. Peng, Y. Zhang, Z. Cheng and J. Lin, *Dalton Trans*., 2012, **41**, 3078; (b) G. Blasse and B. C. Grabmaier, *Luminescence Materials*, Springer-Verlag, Berlin and Heideberg 1994, ch. 4–5.

20 (a) C. Feldman, *Phys. Rev*., 1960, **117**, 455; (b) N. Zhang, C. Guo, J. Zheng, X. Su and J. Zhao, *J. Mater. Chem. C*, 2014, **2**, 3988; (c) Y. Zhang, X. Kang, D. Geng, M. Shang, Y. Wu, X. Li, H. Lian, Cheng and J. Lin, *Dalton Trans*., 2013, **42**, 14140.